

Measurement of the B^0 meson lifetime with partial reconstruction of $B^0 \rightarrow D^{*-} \pi^+$ and $B^0 \rightarrow D^{*-} \rho^+$ decays

B. Aubert,¹ R. Barate,¹ D. Boutigny,¹ J.-M. Gaillard,¹ A. Hicheur,¹ Y. Karyotakis,¹ J. P. Lees,¹ P. Robbe,¹ V. Tisserand,¹
 A. Zghiche,¹ A. Palano,² A. Pompili,² J. C. Chen,³ N. D. Qi,³ G. Rong,³ P. Wang,³ Y. S. Zhu,³ G. Eigen,⁴ I. Ofte,⁴
 B. Stugu,⁴ G. S. Abrams,⁵ A. W. Borgland,⁵ A. B. Breon,⁵ D. N. Brown,⁵ J. Button-Shafer,⁵ R. N. Cahn,⁵ E. Charles,⁵
 M. S. Gill,⁵ A. V. Gritsan,⁵ Y. Groysman,⁵ R. G. Jacobsen,⁵ R. W. Kadel,⁵ J. Kadyk,⁵ L. T. Kerth,⁵
 Yu. G. Kolomensky,⁵ J. F. Kral,⁵ C. LeClerc,⁵ M. E. Levi,⁵ G. Lynch,⁵ L. M. Mir,⁵ P. J. Oddone,⁵ T. J. Orimoto,⁵ M. Pripstein,⁵
 N. A. Roe,⁵ A. Romosan,⁵ M. T. Ronan,⁵ V. G. Shelkov,⁵ A. V. Telnov,⁵ W. A. Wenzel,⁵ T. J. Harrison,⁶ C. M. Hawkes,⁶
 D. J. Knowles,⁶ S. W. O'Neale,⁶ R. C. Penny,⁶ A. T. Watson,⁶ N. K. Watson,⁶ T. Deppermann,⁷ K. Goetzen,⁷
 H. Koch,⁷ B. Lewandowski,⁷ M. Pelizaeus,⁷ K. Peters,⁷ H. Schmuecker,⁷ M. Steinke,⁷ N. R. Barlow,⁸ W. Bhimji,⁸ J. T. Boyd,⁸
 N. Chevalier,⁸ P. J. Clark,⁸ W. N. Cottingham,⁸ C. Mackay,⁸ F. F. Wilson,⁸ C. Hearty,⁹ T. S. Mattison,⁹ J. A. McKenna,⁹
 D. Thiessen,⁹ S. Jolly,¹⁰ P. Kyberd,¹⁰ A. K. McKemey,¹⁰ V. E. Blinov,¹¹ A. D. Bukin,¹¹ A. R. Buzykaev,¹¹
 V. B. Golubev,¹¹ V. N. Ivanchenko,¹¹ A. A. Korol,¹¹ E. A. Kravchenko,¹¹ A. P. Onuchin,¹¹ S. I. Serednyakov,¹¹
 Yu. I. Skovpen,¹¹ A. N. Yushkov,¹¹ D. Best,¹² M. Chao,¹² D. Kirkby,¹² A. J. Lankford,¹² M. Mandelkern,¹² S. McMahon,¹²
 R. K. Mommsen,¹² D. P. Stoker,¹² C. Buchanan,¹³ H. K. Hadavand,¹⁴ E. J. Hill,¹⁴ D. B. MacFarlane,¹⁴ H. P. Paar,¹⁴
 Sh. Rahatlou,¹⁴ G. Raven,¹⁴ U. Schwanke,¹⁴ V. Sharma,¹⁴ J. W. Berryhill,¹⁵ C. Campagnari,¹⁵ B. Dahmes,¹⁵ N. Kuznetsova,¹⁵
 S. L. Levy,¹⁵ O. Long,¹⁵ A. Lu,¹⁵ M. A. Mazur,¹⁵ J. D. Richman,¹⁵ W. Verkerke,¹⁵ J. Beringer,¹⁶ A. M. Eisner,¹⁶
 M. Grothe,¹⁶ C. A. Heusch,¹⁶ W. S. Lockman,¹⁶ T. Pulliam,¹⁶ T. Schalk,¹⁶ R. E. Schmitz,¹⁶ B. A. Schumm,¹⁶ A. Seiden,¹⁶
 M. Turri,¹⁶ W. Walkowiak,¹⁶ D. C. Williams,¹⁶ M. G. Wilson,¹⁶ J. Albert,¹⁷ E. Chen,¹⁷ G. P. Dubois-Felsmann,¹⁷
 A. Dvoretzki,¹⁷ D. G. Hitlin,¹⁷ I. Narsky,¹⁷ F. C. Porter,¹⁷ A. Ryd,¹⁷ A. Samuel,¹⁷ S. Yang,¹⁷ S. Jayatilake,¹⁸ G. Mancinelli,¹⁸
 B. T. Meadows,¹⁸ M. D. Sokoloff,¹⁸ T. Barillari,¹⁹ F. Blanc,¹⁹ P. Bloom,¹⁹ W. T. Ford,¹⁹ U. Nauenberg,¹⁹ A. Olivas,¹⁹
 P. Rankin,¹⁹ J. Roy,¹⁹ J. G. Smith,¹⁹ W. C. van Hoek,¹⁹ L. Zhang,¹⁹ J. L. Harton,²⁰ T. Hu,²⁰ A. Soffer,²⁰ W. H. Toki,²⁰
 R. J. Wilson,²⁰ J. Zhang,²⁰ D. Altenburg,²¹ T. Brandt,²¹ J. Brose,²¹ T. Colberg,²¹ M. Dickopp,²¹ R. S. Dubitzky,²¹
 A. Hauke,²¹ E. Maly,²¹ R. Müller-Pfefferkorn,²¹ R. Nogowski,²¹ S. Otto,²¹ K. R. Schubert,²¹ R. Schwierz,²¹ B. Spaan,²¹
 L. Wilden,²¹ D. Bernard,²² G. R. Bonneaud,²² F. Brochard,²² J. Cohen-Tanugi,²² S. T'Jampens,²² Ch. Thiebaux,²²
 G. Vasileiadis,²² M. Verderi,²² A. Anjomshoa,²³ R. Bernet,²³ A. Khan,²³ D. Lavin,²³ F. Muheim,²³ S. Playfer,²³
 J. E. Swain,²³ J. Tinslay,²³ M. Falbo,²⁴ C. Borean,²⁵ C. Bozzi,²⁵ L. Piemontese,²⁵ A. Sarti,²⁵ E. Treadwell,²⁶ F. Anulli,^{27,*}
 R. Baldini-Ferrolì,²⁷ A. Calcaterra,²⁷ R. de Sangro,²⁷ D. Falciari,²⁷ G. Finocchiaro,²⁷ P. Patteri,²⁷ I. M. Peruzzi,^{27,*}
 M. Piccolo,²⁷ A. Zallo,²⁷ S. Bagnasco,²⁸ A. Buzzo,²⁸ R. Contri,²⁸ G. Crosetti,²⁸ M. Lo Vetere,²⁸ M. Macri,²⁸ M. R. Monge,²⁸
 S. Passaggio,²⁸ F. C. Pastore,²⁸ C. Patrignani,²⁸ E. Robutti,²⁸ A. Santroni,²⁸ S. Tosi,²⁸ S. Bailey,²⁹ M. Morii,²⁹
 G. J. Grenier,³⁰ U. Mallik,³⁰ J. Cochran,³¹ H. B. Crawley,³¹ J. Lamsa,³¹ W. T. Meyer,³¹ S. Prell,³¹ E. I. Rosenberg,³¹ J. Yi,³¹
 M. Davier,³² G. Grosdidier,³² A. Höcker,³² H. M. Lacker,³² S. Laplace,³² F. Le Diberder,³² V. Lepeltier,³² A. M. Lutz,³²
 T. C. Petersen,³² S. Plaszczynski,³² M. H. Schune,³² L. Tantot,³² G. Wormser,³² R. M. Bionta,³³ V. Brigljević,³³ D. J. Lange,³³
 K. van Bibber,³³ D. M. Wright,³³ A. J. Bevan,³⁴ J. R. Fry,³⁴ E. Gabathuler,³⁴ R. Gamet,³⁴ M. George,³⁴ M. Kay,³⁴
 D. J. Payne,³⁴ R. J. Sloane,³⁴ C. Touramanis,³⁴ M. L. Aspinwall,³⁵ D. A. Bowerman,³⁵ P. D. Dauncey,³⁵ U. Egede,³⁵
 I. Eschrich,³⁵ G. W. Morton,³⁵ J. A. Nash,³⁵ P. Sanders,³⁵ G. P. Taylor,³⁵ J. J. Back,³⁶ G. Bellodi,³⁶ P. Dixon,³⁶ P. F. Harrison,³⁶
 H. W. Shorthouse,³⁶ P. Strother,³⁶ P. B. Vidal,³⁶ G. Cowan,³⁷ H. U. Flaecher,³⁷ S. George,³⁷ M. G. Green,³⁷ A. Kurup,³⁷
 C. E. Marker,³⁷ T. R. McMahon,³⁷ S. Ricciardi,³⁷ F. Salvatore,³⁷ G. Vaitsas,³⁷ M. A. Winter,³⁷ D. Brown,³⁸
 C. L. Davis,³⁸ J. Allison,³⁹ R. J. Barlow,³⁹ A. C. Forti,³⁹ P. A. Hart,³⁹ F. Jackson,³⁹ G. D. Lafferty,³⁹ A. J. Lyon,³⁹ N. Savvas,³⁹
 J. H. Weatherall,³⁹ J. C. Williams,³⁹ A. Farbin,⁴⁰ A. Jawahery,⁴⁰ V. Lillard,⁴⁰ D. A. Roberts,⁴⁰ G. Blaylock,⁴¹
 C. Dallapiccola,⁴¹ K. T. Flood,⁴¹ S. S. Hertzbach,⁴¹ R. Kofler,⁴¹ V. B. Koptchev,⁴¹ T. B. Moore,⁴¹ H. Staengle,⁴¹ S. Willocq,⁴¹
 R. Cowan,⁴² G. Sciolla,⁴² F. Taylor,⁴² R. K. Yamamoto,⁴² M. Milek,⁴³ P. M. Patel,⁴³ F. Palombo,⁴⁴ J. M. Bauer,⁴⁵
 L. Cremaldi,⁴⁵ V. Eschenburg,⁴⁵ R. Kroeger,⁴⁵ J. Reidy,⁴⁵ D. A. Sanders,⁴⁵ D. J. Summers,⁴⁵ H. Zhao,⁴⁵ C. Hast,⁴⁶ P. Taras,⁴⁶
 H. Nicholson,⁴⁷ C. Cartaro,⁴⁸ N. Cavallo,⁴⁸ G. De Nardo,⁴⁸ F. Fabozzi,^{48,†} C. Gatto,⁴⁸ L. Lista,⁴⁸ P. Paolucci,⁴⁸
 D. Piccolo,⁴⁸ C. Sciacca,⁴⁸ J. M. LoSecco,⁴⁹ J. R. G. Alsmiller,⁵⁰ T. A. Gabriel,⁵⁰ B. Brau,⁵¹ J. Brau,⁵² R. Frey,⁵² M. Iwasaki,⁵²
 C. T. Potter,⁵² N. B. Sinev,⁵² D. Strom,⁵² E. Torrence,⁵² F. Colecchia,⁵³ A. Dorigo,⁵³ F. Galeazzi,⁵³ M. Margoni,⁵³
 M. Morandin,⁵³ M. Posocco,⁵³ M. Rotondo,⁵³ F. Simonetto,⁵³ R. Stroili,⁵³ G. Tiozzo,⁵³ C. Voci,⁵³ M. Benayoun,⁵⁴ H. Briand,⁵⁴
 J. Chauveau,⁵⁴ P. David,⁵⁴ Ch. de la Vaissière,⁵⁴ L. Del Buono,⁵⁴ O. Hamon,⁵⁴ Ph. Leruste,⁵⁴ J. Ocariz,⁵⁴ M. Pivk,⁵⁴
 L. Roos,⁵⁴ J. Stark,⁵⁴ P. F. Manfredi,⁵⁵ V. Re,⁵⁵ V. Speziali,⁵⁵ L. Gladney,⁵⁶ Q. H. Guo,⁵⁶ J. Panetta,⁵⁶ C. Angelini,⁵⁷
 G. Batignani,⁵⁷ S. Bettarini,⁵⁷ M. Bondioli,⁵⁷ F. Bucci,⁵⁷ G. Calderini,⁵⁷ E. Campagna,⁵⁷ M. Carpinelli,⁵⁷ F. Forti,⁵⁷
 M. A. Giorgi,⁵⁷ A. Lusiani,⁵⁷ G. Marchiori,⁵⁷ F. Martinez-Vidal,⁵⁷ M. Morganti,⁵⁷ N. Neri,⁵⁷ E. Paoloni,⁵⁷ M. Rama,⁵⁷
 G. Rizzo,⁵⁷ F. Sandrelli,⁵⁷ G. Triggiani,⁵⁷ J. Walsh,⁵⁷ M. Haire,⁵⁸ D. Judd,⁵⁸ K. Paick,⁵⁸ L. Turnbull,⁵⁸
 D. E. Wagoner,⁵⁸ N. Danielson,⁵⁹ P. Elmer,⁵⁹ C. Lu,⁵⁹ V. Miftakov,⁵⁹ J. Olsen,⁵⁹ A. J. S. Smith,⁵⁹ A. Tumanov,⁵⁹
 E. W. Varnes,⁵⁹ F. Bellini,⁶⁰ G. Cavoto,^{59,60} D. del Re,⁶⁰ R. Faccini,⁶⁰ F. Ferrarotto,⁶⁰ F. Ferroni,⁶⁰ M. Gaspero,⁶⁰
 E. Leonardi,⁶⁰ M. A. Mazzoni,⁶⁰ S. Morganti,⁶⁰ G. Piredda,⁶⁰ F. Safai Tehrani,⁶⁰ M. Serra,⁶⁰ C. Voena,⁶⁰ S. Christ,⁶¹
 G. Wagner,⁶¹ R. Waldi,⁶¹ T. Adye,⁶² N. De Groot,⁶² B. Franek,⁶² N. I. Geddes,⁶² G. P. Gopal,⁶² E. O. Olaiya,⁶² S. M. Xella,⁶²
 R. Aleksan,⁶³ S. Emery,⁶³ A. Gaidot,⁶³ P.-F. Giraud,⁶³ G. Hamel de Monchenault,⁶³ W. Kozanecki,⁶³ M. Langer,⁶³

G. W. London,⁶³ B. Mayer,⁶³ G. Schott,⁶³ B. Serfass,⁶³ G. Vasseur,⁶³ Ch. Yeche,⁶³ M. Zito,⁶³ M. V. Purohit,⁶⁴ F. X. Yumiceva,⁶⁴ A. W. Weidemann,⁶⁴ K. Abe,⁶⁵ D. Aston,⁶⁵ R. Bartoldus,⁶⁵ N. Berger,⁶⁵ A. M. Boyarski,⁶⁵ O. L. Buchmueller,⁶⁵ M. R. Convery,⁶⁵ D. P. Coupal,⁶⁵ D. Dong,⁶⁵ J. Dorfan,⁶⁵ W. Dunwoodie,⁶⁵ R. C. Field,⁶⁵ T. Glanzman,⁶⁵ S. J. Gowdy,⁶⁵ E. Grauges-Pous,⁶⁵ T. Hadig,⁶⁵ V. Halyo,⁶⁵ T. Himel,⁶⁵ T. Hryn'ova,⁶⁵ M. E. Huffer,⁶⁵ W. R. Innes,⁶⁵ C. P. Jessop,⁶⁵ M. H. Kelsey,⁶⁵ P. Kim,⁶⁵ M. L. Kocian,⁶⁵ U. Langenegger,⁶⁵ D. W. G. S. Leith,⁶⁵ S. Luitz,⁶⁵ V. Luth,⁶⁵ H. L. Lynch,⁶⁵ H. Marsiske,⁶⁵ S. Menke,⁶⁵ R. Messner,⁶⁵ D. R. Muller,⁶⁵ C. P. O'Grady,⁶⁵ V. E. Ozcan,⁶⁵ A. Perazzo,⁶⁵ M. Perl,⁶⁵ S. Petrak,⁶⁵ B. N. Ratcliff,⁶⁵ S. H. Robertson,⁶⁵ A. Roodman,⁶⁵ A. A. Salnikov,⁶⁵ T. Schietinger,⁶⁵ R. H. Schindler,⁶⁵ J. Schwiening,⁶⁵ G. Simi,⁶⁵ A. Snyder,⁶⁵ A. Soha,⁶⁵ J. Stelzer,⁶⁵ D. Su,⁶⁵ M. K. Sullivan,⁶⁵ H. A. Tanaka,⁶⁵ J. Va'vra,⁶⁵ S. R. Wagner,⁶⁵ M. Weaver,⁶⁵ A. J. R. Weinstein,⁶⁵ W. J. Wisniewski,⁶⁵ D. H. Wright,⁶⁵ C. C. Young,⁶⁵ P. R. Burchat,⁶⁶ C. H. Cheng,⁶⁶ T. I. Meyer,⁶⁶ C. Roat,⁶⁶ W. Bugg,⁶⁷ M. Krishnamurthy,⁶⁷ S. M. Spanier,⁶⁷ J. M. Izen,⁶⁸ I. Kitayama,⁶⁸ X. C. Lou,⁶⁸ F. Bianchi,⁶⁹ M. Bona,⁶⁹ D. Gamba,⁶⁹ L. Bosisio,⁷⁰ G. Della Ricca,⁷⁰ S. Dittongo,⁷⁰ L. Lanceri,⁷⁰ P. Poropat,⁷⁰ L. Vitale,⁷⁰ G. Vuagnin,⁷⁰ R. Henderson,⁷¹ R. S. Panvini,⁷² Sw. Banerjee,⁷³ C. M. Brown,⁷³ D. Fortin,⁷³ P. D. Jackson,⁷³ R. Kowalewski,⁷³ J. M. Roney,⁷³ H. R. Band,⁷⁴ S. Dasu,⁷⁴ M. Datta,⁷⁴ A. M. Eichenbaum,⁷⁴ H. Hu,⁷⁴ J. R. Johnson,⁷⁴ R. Liu,⁷⁴ F. Di Lodovico,⁷⁴ A. K. Mohapatra,⁷⁴ Y. Pan,⁷⁴ R. Prepost,⁷⁴ S. J. Sekula,⁷⁴ J. H. von Wimmersperg-Toeller,⁷⁴ J. Wu,⁷⁴ S. L. Wu,⁷⁴ Z. Yu,⁷⁴ and H. Neal⁷⁵

(BABAR Collaboration)

¹Laboratoire de Physique des Particules, F-74941 Annecy-le-Vieux, France²Università di Bari, Dipartimento di Fisica and INFN, I-70126 Bari, Italy³Institute of High Energy Physics, Beijing 100039, China⁴University of Bergen, Inst. of Physics, N-5007 Bergen, Norway⁵Lawrence Berkeley National Laboratory and University of California, Berkeley, California 94720, USA⁶University of Birmingham, Birmingham, B15 2TT, United Kingdom⁷Ruhr Universität Bochum, Institut für Experimentalphysik 1, D-44780 Bochum, Germany⁸University of Bristol, Bristol BS8 1TL, United Kingdom⁹University of British Columbia, Vancouver, British Columbia, Canada V6T 1Z1¹⁰Brunel University, Uxbridge, Middlesex UB8 3PH, United Kingdom¹¹Budker Institute of Nuclear Physics, Novosibirsk 630090, Russia¹²University of California at Irvine, Irvine, California 92697, USA¹³University of California at Los Angeles, Los Angeles, California 90024, USA¹⁴University of California at San Diego, La Jolla, California 92093, USA¹⁵University of California at Santa Barbara, Santa Barbara, California 93106, USA¹⁶University of California at Santa Cruz, Institute for Particle Physics, Santa Cruz, California 95064, USA¹⁷California Institute of Technology, Pasadena, California 91125, USA¹⁸University of Cincinnati, Cincinnati, Ohio 45221, USA¹⁹University of Colorado, Boulder, Colorado 80309, USA²⁰Colorado State University, Fort Collins, Colorado 80523, USA²¹Technische Universität Dresden, Institut für Kern- und Teilchenphysik, D-01062 Dresden, Germany²²Ecole Polytechnique, LLR, F-91128 Palaiseau, France²³University of Edinburgh, Edinburgh EH9 3JZ, United Kingdom²⁴Elon University, Elon University, North Carolina 27244-2010, USA²⁵Università di Ferrara, Dipartimento di Fisica and INFN, I-44100 Ferrara, Italy²⁶Florida A&M University, Tallahassee, Florida 32307, USA²⁷Laboratori Nazionali di Frascati dell'INFN, I-00044 Frascati, Italy²⁸Università di Genova, Dipartimento di Fisica and INFN, I-16146 Genova, Italy²⁹Harvard University, Cambridge, Massachusetts 02138, USA³⁰University of Iowa, Iowa City, Iowa 52242, USA³¹Iowa State University, Ames, Iowa 50011-3160, USA³²Laboratoire de l'Accélérateur Linéaire, F-91898 Orsay, France³³Lawrence Livermore National Laboratory, Livermore, California 94550, USA³⁴University of Liverpool, Liverpool L69 3BX, United Kingdom³⁵University of London, Imperial College, London, SW7 2BW, United Kingdom³⁶Queen Mary, University of London, E1 4NS, United Kingdom³⁷University of London, Royal Holloway and Bedford New College, Egham, Surrey TW20 0EX, United Kingdom³⁸University of Louisville, Louisville, Kentucky 40292, USA³⁹University of Manchester, Manchester M13 9PL, United Kingdom⁴⁰University of Maryland, College Park, Maryland 20742, USA⁴¹University of Massachusetts, Amherst, Massachusetts 01003, USA⁴²Massachusetts Institute of Technology, Laboratory for Nuclear Science, Cambridge, Massachusetts 02139, USA

- ⁴³McGill University, Montréal Quebec, Canada H3A 2T8
⁴⁴Università di Milano, Dipartimento di Fisica and INFN, I-20133 Milano, Italy
⁴⁵University of Mississippi, University, Mississippi 38677, USA
⁴⁶Université de Montréal, Laboratoire René J. A. Lévesque, Montréal, Quebec, Canada H3C 3J7
⁴⁷Mount Holyoke College, South Hadley, Massachusetts 01075, USA
⁴⁸Università di Napoli Federico II, Dipartimento di Scienze Fisiche and INFN, I-80126, Napoli, Italy
⁴⁹University of Notre Dame, Notre Dame, Indiana 46556, USA
⁵⁰Oak Ridge National Laboratory, Oak Ridge, Tennessee 37831, USA
⁵¹Ohio State University, 174 West 18th Avenue, Columbus, Ohio 43210, USA
⁵²University of Oregon, Eugene, Oregon 97403, USA
⁵³Università di Padova, Dipartimento di Fisica and INFN, I-35131 Padova, Italy
⁵⁴Universités Paris VI et VII, Lab de Physique Nucléaire H. E., F-75252 Paris, France
⁵⁵Università di Pavia, Dipartimento di Elettronica and INFN, I-27100 Pavia, Italy
⁵⁶University of Pennsylvania, Philadelphia, Pennsylvania 19104, USA
⁵⁷Università di Pisa, Scuola Normale Superiore and INFN, I-56010 Pisa, Italy
⁵⁸Prairie View A&M University, Prairie View, Texas 77446, USA
⁵⁹Princeton University, Princeton, New Jersey 08544, USA
⁶⁰Università di Roma La Sapienza, Dipartimento di Fisica and INFN, I-00185 Roma, Italy
⁶¹Universität Rostock, D-18051 Rostock, Germany
⁶²Rutherford Appleton Laboratory, Chilton, Didcot, Oxon, OX11 0QX, United Kingdom
⁶³DAPNIA, Commissariat à l'Energie Atomique/Saclay, F-91191 Gif-sur-Yvette, France
⁶⁴University of South Carolina, Columbia, South Carolina 29208, USA
⁶⁵Stanford Linear Accelerator Center, Stanford, California 94309, USA
⁶⁶Stanford University, Stanford, California 94305-4060, USA
⁶⁷University of Tennessee, Knoxville, Tennessee 37996, USA
⁶⁸University of Texas at Dallas, Richardson, Texas 75083, USA
⁶⁹Università di Torino, Dipartimento di Fisica Sperimentale and INFN, I-10125 Torino, Italy
⁷⁰Università di Trieste, Dipartimento di Fisica and INFN, I-34127 Trieste, Italy
⁷¹TRIUMF, Vancouver, British Columbia, Canada V6T 2A3
⁷²Vanderbilt University, Nashville, Tennessee 37235, USA
⁷³University of Victoria, Victoria, British Columbia, Canada V8W 3P6
⁷⁴University of Wisconsin, Madison, Wisconsin 53706, USA
⁷⁵Yale University, New Haven, Connecticut 06511, USA

(Received 5 December 2002; published 20 May 2003)

The neutral B meson lifetime is measured with the data collected by the $BABAR$ detector at the PEP-II storage ring during the years 1999 and 2000, with a total integrated luminosity of 20.7 fb^{-1} . The decays $B^0 \rightarrow D^{*-} \pi^+$ and $B^0 \rightarrow D^{*-} \rho^+$ are selected with a partial-reconstruction technique, yielding samples of 6970 ± 240 and 5520 ± 250 signal events, respectively. With these events, the B^0 lifetime is measured to be $1.533 \pm 0.034 \text{ (stat)} \pm 0.038 \text{ (syst) ps}$. This measurement serves as a test and validation of procedures required to measure the CP violation parameter $\sin(2\beta + \gamma)$ with partial reconstruction of these modes.

DOI: 10.1103/PhysRevD.67.091101

PACS number(s): 13.25.Hw, 11.30.Er, 12.15.Hh

The neutral B meson decay modes [1] $B^0 \rightarrow D^{*-} h^+$, where h^+ is a light hadron (π^+, ρ^+, a_1^+), have been proposed for use in theoretically clean measurements of $\sin(2\beta + \gamma)$ [2], where $(2\beta + \gamma)$ is a combination of angles of the Cabibbo-Kobayashi-Maskawa [3] unitarity triangle. Since the time-dependent CP asymmetries in these modes are expected to be of order 2%, large data samples and multiple decay channels are required for a statistically significant measurement. The technique of partial reconstruction of D^{*-} mesons, in which only the soft pion π_s from the decay $D^{*-} \rightarrow \bar{D}^0 \pi_s^-$ is reconstructed, has already been used to se-

lect large samples of B meson candidates [4]. This technique is applied here to the decays $B^0 \rightarrow D^{*-} \pi^+$ and $B^0 \rightarrow D^{*-} \rho^+$ in order to measure the B^0 lifetime. In addition to providing a measurement of the lifetime, this analysis constitutes a first step toward measuring $\sin(2\beta + \gamma)$, validating the procedures developed for candidate reconstruction, background characterization, vertex reconstruction, and fitting of decay time distributions. These procedures address the main complications introduced by partial reconstruction, namely the large background and the tracks originating from the unreconstructed \bar{D}^0 , which may affect the vertex reconstruction.

The analyses applied to the $B^0 \rightarrow D^{*-} \pi^+$ and $B^0 \rightarrow D^{*-} \rho^+$ modes are similar. Detailed differences between them are the result of optimization in the presence of the

*Also with Università di Perugia, Perugia, Italy.

†Also with Università della Basilicata, Potenza, Italy.

different background characteristics in the two modes. Additional details regarding the analysis procedures can be found in Refs. [5] and [6].

The data used in this analysis were collected with the *BABAR* detector at the SLAC e^+e^- asymmetric-energy storage ring PEP-II during the years 1999 and 2000. The data consist of 22.7 million $B\bar{B}$ pairs, corresponding to an integrated luminosity of 20.7 fb^{-1} recorded at the $\Upsilon(4S)$ resonance. In addition, 2.6 fb^{-1} of “off-resonance” data were collected about 40 MeV below the resonance. Samples of simulated $B\bar{B}$ and continuum $e^+e^- \rightarrow q\bar{q}$ events, where q stands for a u , d , s , or c quark, were generated using a GEANT3-based detector simulation [7] and processed through the same reconstruction and analysis chain as the data. The equivalent luminosity of the simulated events is approximately one third the data luminosity. We also used signal Monte Carlo samples with an equivalent luminosity several times larger than that of the data.

The *BABAR* detector, described in detail elsewhere [8], consists of five subdetectors. Charged particle trajectories are measured by a combination of a five-layer silicon vertex tracker (SVT) and a 40-layer drift chamber (DCH) in a 1.5 T solenoidal magnetic field. Tracks with low transverse momentum are reconstructed by the SVT alone, thus extending the charged particle detection down to transverse momenta of $\sim 50 \text{ MeV}/c$. Photons and electrons are detected in a CsI(Tl) electromagnetic calorimeter (EMC), with photon energy resolution $\sigma_E/E = 0.023(E/\text{GeV})^{-1/4} \oplus 0.019$. A ring-imaging Cherenkov detector (DIRC) is used for charged particle identification. The instrumented flux return (IFR) is equipped with resistive plate chambers to identify muons.

In the partial reconstruction of a $B^0 \rightarrow D^{*-} h^+$ candidate, only the hadron h and the π_s are reconstructed. The angle between the momenta of the B and the h in the center-of-mass (c.m.) frame is then computed:

$$\cos \theta_{Bh} = \frac{M_{D^{*-}}^2 - M_{B^0}^2 - M_h^2 + E_{\text{CM}} E_h}{2p_B |\vec{p}_h|}, \quad (1)$$

where M_x is the mass of particle x , E_h and \vec{p}_h are the measured c.m. energy and momentum of the hadron h , $E_{\text{c.m.}}$ is the total c.m. energy of the beams, and $p_B = \sqrt{E_{\text{CM}}^2/4 - M_{B^0}^2}$. All masses M_x refer to the nominal values [9], except in the case $h = \rho$, where the measured $\pi^+ \pi^0$ invariant mass $m(\pi^+ \pi^0)$ is used. Events are required to be in the physical region $|\cos \theta_{Bh}| < 1$. Given p_B , $\cos \theta_{Bh}$, and \vec{p}_h , the B four-momentum can be calculated up to an unknown azimuthal angle ϕ around \vec{p}_h . For every value of ϕ , one may use four-momentum conservation to determine the expected \bar{D}^0 four-momentum $\mathcal{P}_D(\phi) = \mathcal{P}_B(\phi) - \mathcal{P}_h - \mathcal{P}_{\pi_s}$, where \mathcal{P}_x is the four-momentum of particle x . The corresponding ϕ -dependent \bar{D}^0 invariant mass is $m(\phi) \equiv \sqrt{|\mathcal{P}_D(\phi)|^2}$. We define the missing mass $m_{\text{miss}} \equiv 1/2[m_{\text{max}} + m_{\text{min}}]$, where m_{max} and m_{min} are the maximum and minimum values that $m(\phi)$ may obtain given the momenta of h and π_s . In signal events, m_{miss} peaks at the nominal \bar{D}^0 mass M_{D^0} , with a spread of about $3 \text{ MeV}/c^2$ for $B^0 \rightarrow D^{*-} \pi^+$

($3.5 \text{ MeV}/c^2$ for $B^0 \rightarrow D^{*-} \rho^+$) [10], while the distribution of background events is broader. The missing mass is the main variable used to distinguish signal from background.

We define the D^* helicity angle θ_{D^*} to be the angle between the directions of the \bar{D}^0 and the B^0 in the D^* rest frame. This variable is used in the event selection described below. In the $B^0 \rightarrow D^{*-} \pi^+$ analysis, θ_{D^*} is computed assuming that the B momentum lies in the plane defined by the h and π_s momenta in the c.m. frame. This assumption also yields the \bar{D}^0 direction. In the $B^0 \rightarrow D^{*-} \rho^+$ analysis, the value of $\cos \theta_{D^*}$ is computed by applying the constraint $m_{\text{miss}} = M_{D^0}$ giving two possible solutions for the \bar{D}^0 direction [4]. In $B^0 \rightarrow D^{*-} \rho^+$, the ρ helicity angle θ_ρ is defined as the angle between the directions of the π^0 (from the decay of the ρ) and the c.m. system in the ρ rest frame.

We select events in which the ratio of the 2nd to the 0th Fox-Wolfram moment [11], computed using charged particles, is smaller than 0.35. The candidate B^0 daughter tracks are required to originate within 1 cm (1.5 cm) of the interaction point in the x - y plane (the plane perpendicular to the beams), and within ± 4 cm (± 10 cm) of the interaction point along the direction of the beams. Tracks are rejected if they are highly likely to be a kaon or a lepton on the basis of their ionization, Cherenkov angle, energy deposited in the EMC, and pattern of hits in the IFR.

$B^0 \rightarrow D^{*-} \pi^+$ candidates are rejected if another track is found within 0.4 rad of the momentum of the hard pion π_h [12] in the c.m. frame. This requirement helps to reject continuum events, where tracks tend to be clustered in jets. A Fisher discriminant [13] F_π is computed from 15 event shape variables. Among these variables is the scalar sum of the c.m. momenta of all tracks and neutral candidates in nine 20° single-sided cones around the π_h direction. We require $|\cos \theta_{D^*}|$ to be larger than 0.4. A cut on F_π is used to reduce the continuum background.

In the reconstruction of $B^0 \rightarrow D^{*-} \rho^+$ candidates, the charged ρ candidates are identified by their decay to a hard charged pion π_h and a π^0 . To suppress fake π^0 candidates, the π^0 momentum in the c.m. frame is required to be greater than $400 \text{ MeV}/c$. The invariant mass of the $\pi^0 \rightarrow \gamma\gamma$ candidate must be within $20 \text{ MeV}/c^2$ of the nominal π^0 mass [9]. The invariant mass $m(\pi^+ \pi^0)$ of the ρ candidate must be between 0.45 and $1.10 \text{ GeV}/c^2$. To suppress combinatoric background, we require $|\cos \theta_\rho| > 0.3$ and $|\cos \theta_{D^*}| > 0.3$, and also reject events that satisfy both $\cos \theta_\rho > 0.3$ and $\cos \theta_{D^*} < -0.3$. A Fisher discriminant F_ρ is computed using the scalar sum of the c.m. momenta of all tracks and neutrals in nine 10° double-sided cones around the ρ direction. In about 10% of the events, more than one partially reconstructed candidate per event satisfies all the requirements, in good agreement with what is observed in Monte Carlo simulated events. In such events only the candidate with the smallest value of $|m_{\text{miss}} - M_{D^0}|$ in the event is used.

The decay position z_{rec} of the partially reconstructed B candidate along the beam direction is determined by constraining the π_h and the π_s tracks (only the π_h track for $B^0 \rightarrow D^{*-} \rho^+$) to originate from the beam-spot in the x - y plane. The beam spot is determined on a run-by-run basis

using two-prong events [8]. Its size in the horizontal direction is $120 \mu\text{m}$. Although the beam spot size in the vertical direction is only a few microns, a beam spot constraint of $30 \mu\text{m}$ is applied, so as to account for the flight of the B^0 in the vertical direction.

The decay position z_{other} of the other B meson along the beam direction is measured with all tracks, excluding π_h , π_s , and any track whose c.m. angle with respect to the \bar{D}^0 direction (either of the two calculated directions in the $B^0 \rightarrow D^{*-} \rho^+$ case) is smaller than 1 radian. This ‘‘cone cut’’ reduces the fraction of events in which \bar{D}^0 daughter tracks are used in the other B vertex to about 25%, while maintaining high vertex fit efficiency. The tracks satisfying this requirement are fit with a constraint to the beam-spot in the $x-y$ plane. The track with the largest contribution to the χ^2 of the vertex, if greater than 6, is removed from the vertex, and the fit is carried out again, until no track fails this requirement. $B^0 \rightarrow D^{*-} \pi^+$ candidates are required to have at least two tracks remaining in the other B vertex.

The z distance between the two B decay vertices, $\Delta z = z_{\text{rec}} - z_{\text{other}}$, is computed. Fitting the residual $\Delta z - \Delta z_{\text{true}}$ in simulated events, where Δz_{true} is the true Δz , with the sum of two Gaussians, we find that 67% (57%) of the $B^0 \rightarrow D^{*-} \pi^+$ ($B^0 \rightarrow D^{*-} \rho^+$) events lie in the core Gaussian of width $116 \mu\text{m}$ ($178 \mu\text{m}$). The Δz resolution is dominated by the measurement of z_{other} , and by the z_{rec} measurement when the π_h transverse momentum is below about $400 \text{ MeV}/c$.

The decay time difference Δt is then calculated using the approximation $\Delta t \approx \Delta z / (\gamma\beta c)$, where the c.m. frame boost $\gamma\beta$ is determined from the beam energies, and has an average value of 0.55. This approximation results in a 0.2 ps rms spread in the calculation of Δt .

For $B^0 \rightarrow D^{*-} \pi^+$ candidates, Δt is computed applying an event-by-event correction to the measured value of Δz . This correction, determined from the simulated signal sample as a function of Δz , removes the bias in z_{other} due to the tracks coming from the \bar{D}^0 decay. Without correction, the effect of this bias would be to reduce the measured lifetime by approximately 4%. In the $B^0 \rightarrow D^{*-} \rho^+$ analysis a different correction is applied to the measured lifetime value, as explained later.

The estimated error $\sigma_{\Delta t}$ in the measurement of Δt is calculated from the uncertainties in the parameters of the tracks used in the two vertex fits. A requirement on the vertex fit probabilities removes badly reconstructed vertices. For both modes we also require $|\Delta t| < 15 \text{ ps}$ and $\sigma_{\Delta t} < 2.4 \text{ ps}$ ($\sigma_{\Delta t} < 4 \text{ ps}$ for $B^0 \rightarrow D^{*-} \rho^+$).

After applying all the above requirements, we find four broadly defined types of events that contribute to the background: (1) Combinatoric $B\bar{B}$ background due to random h and π_s combinations; (2) peaking $B\bar{B}$ events, which are distributed as a broad peak in the m_{miss} spectrum; (3) $B^0 \rightarrow D^{*-} \rho^+$ ($B^0 \rightarrow D^{*-} a_1^+$) decays in the $B^0 \rightarrow D^{*-} \pi^+$ ($B^0 \rightarrow D^{*-} \rho^+$) sample; (4) continuum events. The peaking background is mostly due to $B \rightarrow D^{**} \pi$ decays in the $B^0 \rightarrow D^{*-} \pi^+$ sample. In the $B^0 \rightarrow D^{*-} \rho^+$ sample, it is due to signal events in which the π_h candidate originates from the other B .

The lifetime τ_{B^0} is obtained from an unbinned maximum likelihood fit, as described below, with a probability density function (PDF) $\mathcal{F}(\Delta t, \sigma_{\Delta t}, \xi)$. Here ξ refers to the kinematic variables used to distinguish signal from background. For $B^0 \rightarrow D^{*-} \pi^+$ we set $\xi = m_{\text{miss}}$; for $B^0 \rightarrow D^{*-} \rho^+$ we set $\xi = (m_{\text{miss}}, m(\pi^+ \pi^0), F_\rho)$. The PDF has the form

$$\begin{aligned} \mathcal{F}(\xi, \Delta t, \sigma_{\Delta t}) = & f_{\text{sig}} \mathcal{K}_{\text{sig}}(\xi) \mathcal{F}_{\text{sig}}(\Delta t, \sigma_{\Delta t}) \\ & + f_{\text{comb}} \mathcal{K}_{\text{comb}}(\xi) \mathcal{F}_{\text{comb}}(\Delta t, \sigma_{\Delta t}) \\ & + f_{\text{peak}} \mathcal{K}_{\text{peak}}(\xi) \mathcal{F}_{\text{peak}}(\Delta t, \sigma_{\Delta t}) \\ & + f_{D^*X} \mathcal{K}_{D^*X}(\xi) \mathcal{F}_{D^*X}(\Delta t, \sigma_{\Delta t}) \\ & + f_{\text{cont}} \mathcal{K}_{\text{cont}}(\xi) \mathcal{F}_{\text{cont}}(\Delta t, \sigma_{\Delta t}), \end{aligned} \quad (2)$$

where the subscripts sig, comb, peak, D^*X , and cont refer to the four types of backgrounds enumerated above and to signal events. For each event type i , f_i is the relative population of these events in the data sample, $\mathcal{K}_i(\xi)$ is their kinematic-variables PDF, and $\mathcal{F}_i(\Delta t, \sigma_{\Delta t})$ is their time-dependent PDF. The constraint $\sum f_i = 1$ is enforced.

For $B^0 \rightarrow D^{*-} \pi^+$, $\mathcal{K}_i(m_{\text{miss}})$ consists of binned histograms obtained from the Monte Carlo simulation. For $B^0 \rightarrow D^{*-} \rho^+$ candidates, we use the product $\mathcal{K}_i(\xi) = \mathcal{M}_i(m_{\text{miss}}) \mathcal{R}_i(m(\pi^+ \pi^0)) \mathcal{D}_i(F_\rho)$, where $\mathcal{M}_i(m_{\text{miss}})$ is the sum of a bifurcated Gaussian and an ARGUS function [14], $\mathcal{R}_i(m(\pi^+ \pi^0))$ is the sum of a parabolic background and a relativistic P -wave Breit-Wigner, and $\mathcal{D}_i(F_\rho)$ is a bifurcated Gaussian function.

For each event type i , $\mathcal{F}_i(\Delta t, \sigma_{\Delta t})$ is the convolution $N \int P(\Delta t_{\text{true}}) R((\Delta t - \Delta t_{\text{true}}) / \sigma_{\Delta t}) d\Delta t_{\text{true}}$ of the ‘‘true’’ distribution $P(\Delta t_{\text{true}})$ and the detector resolution function $R((\Delta t - \Delta t_{\text{true}}) / \sigma_{\Delta t})$, which is parametrized as the sum of three Gaussian distributions. N is a normalization constant. The parameters of $P(\Delta t_{\text{true}})$ and $R((\Delta t - \Delta t_{\text{true}}) / \sigma_{\Delta t})$ are obtained separately for each event type. For signal events of both modes we take $P(\Delta t_{\text{true}}) = (1/2\tau_{B^0}) e^{-|\Delta t_{\text{true}}|/\tau_{B^0}}$. This functional form is also used for the combinatoric and peaking backgrounds in $B^0 \rightarrow D^{*-} \pi^+$, but with independent parameters. In $B^0 \rightarrow D^{*-} \rho^+$, the source of the peaking background motivates its distribution to be $P(\Delta t_{\text{true}}) = \delta(\Delta t_{\text{true}})$, and the distribution used for the combinatoric background is $P(\Delta t_{\text{true}}) = a(1/2\tau') e^{-|\Delta t_{\text{true}}|/\tau'} + (1-a)\delta(\Delta t_{\text{true}})$, with an effective lifetime parameter τ' . $\mathcal{F}_{D^*X}(\Delta t, \sigma_{\Delta t})$ is assumed to be identical to $\mathcal{F}_{\text{sig}}(\Delta t, \sigma_{\Delta t})$. The continuum background is modelled as $P(\Delta t_{\text{true}}) = b(1/2\tau_{\text{cont}}) e^{-|\Delta t_{\text{true}}|/\tau_{\text{cont}}} + (1-b)\delta(\Delta t_{\text{true}})$. The validity of these PDFs and corresponding assumptions are individually verified using the Monte Carlo simulation.

Several subsamples are defined and used in the lifetime fit. Events with a candidate in which the h and π_s have opposite charges and with $m_{\text{miss}} > 1.860 \text{ GeV}/c^2$ ($m_{\text{miss}} > 1.845 \text{ GeV}/c^2$ in $B^0 \rightarrow D^{*-} \rho^+$) constitute the ‘‘signal region’’ sample. Those satisfying $1.820 < m_{\text{miss}} < 1.850 \text{ GeV}/c^2$ ($1.810 < m_{\text{miss}} < 1.840 \text{ GeV}/c^2$) constitute the ‘‘sideband.’’ Events in which h and π_s have the same charge are labeled as ‘‘same charge.’’ In the $B^0 \rightarrow D^{*-} \pi^+$ analysis, we apply a requirement on the Fisher discriminant

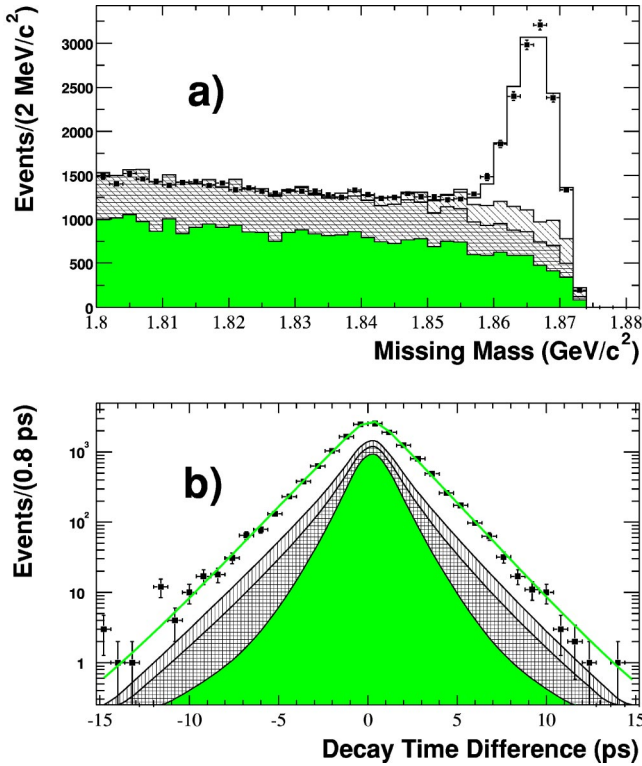


FIG. 1. Distributions of (a) missing mass and (b) Δt for candidate $B^0 \rightarrow D^{*-} \pi^+$ events. The result of the fit (solid line) is superimposed on data (data points). The hatched, cross-hatched, and shaded areas are the peaking $B\bar{B}$, combinatoric $B\bar{B}$, and continuum contributions, respectively. The Δt plot is obtained with the requirement $m_{\text{miss}} > 1.860 \text{ GeV}/c^2$.

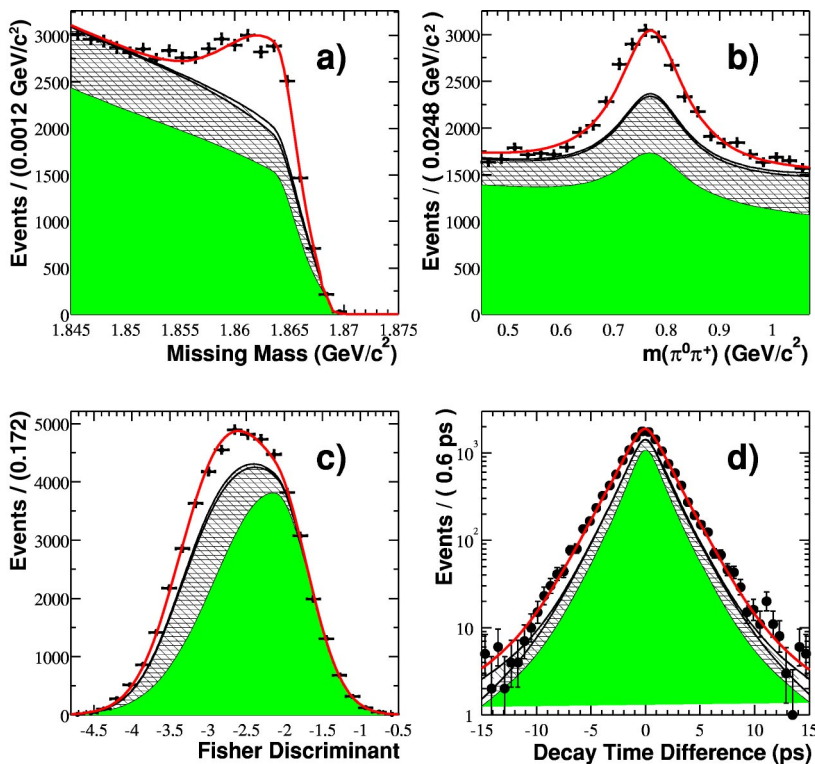


FIG. 2. Distributions of (a) missing mass, (b) ρ candidate invariant mass, (c) Fisher discriminant F_ρ , and (d) Δt of $B^0 \rightarrow D^{*-} \rho^+$ candidate events. The result of the fit (solid line) is superimposed on data (data points). The hatched, cross-hatched, and shaded areas are the peaking $B\bar{B}$, combinatoric $B\bar{B}$, and continuum contributions, respectively. The Δt plot is obtained with the requirement $m_{\text{miss}} > 1.854 \text{ GeV}/c^2$, $0.60 < m(\pi^+\pi^0) < 0.93 \text{ GeV}/c^2$, and $F_\rho < -2.1$.

that suppresses $B\bar{B}$ events, to select a “ $B\bar{B}$ -depleted” sample that is enriched in continuum events. The sideband, same-charge, and $B\bar{B}$ -depleted samples serve as control samples for studying the Δt distributions of the backgrounds.

In the $B^0 \rightarrow D^{*-} \rho^+$ analysis, about 11.5% of the partially reconstructed signal events are also fully reconstructed in the \bar{D}^0 decay modes $\bar{D}^0 \rightarrow K^+ \pi^-$ or $K^+ \pi^- \pi^0$. This yields a sample that, while relatively small, has a low background contamination of about 5%. This clean signal sample is used in the fits described below, improving the determination of the signal PDF parameters.

The B^0 lifetime τ_{B^0} is obtained in a three-step procedure using signal region and control sample events.

In the first step, the fractions f_i in the signal region and in the different control samples are obtained from kinematic-variable fits conducted simultaneously on the on- and off-resonance samples (and the fully reconstructed sample for the $B^0 \rightarrow D^{*-} \rho^+$ signal region). The fit PDF is that of Eq. (2), but with all $\mathcal{F}_i(\Delta t, \sigma_{\Delta t})$ replaced by unity. In the $B^0 \rightarrow D^{*-} \pi^+$ analysis this fit determines f_{peak} and f_{cont} . The fraction of $B^0 \rightarrow D^{*-} \rho^+$ events f_{D^*X} in the $B^0 \rightarrow D^{*-} \pi^+$ sample is assumed to be 16.8%, as predicted by the Monte Carlo simulation and the relative branching ratio [9]. This fit [Fig. 1(a)] yields 6970 ± 240 signal $B^0 \rightarrow D^{*-} \pi^+$ events. In the $B^0 \rightarrow D^{*-} \rho^+$ analysis the kinematic-variable fit determines f_{cont} , as well as all the parameters of $\mathcal{K}_{\text{cont}}(\xi)$, $\mathcal{M}_{\text{sig}}(m_{\text{miss}})$, and $\mathcal{R}_{\text{sig}}(m(\pi^+\pi^0))$. The parameters of $\mathcal{D}_{\text{sig}}(F_\rho)$, $\mathcal{K}_{\text{comb}}(\xi)$, and $\mathcal{K}_{\text{peak}}(\xi)$, as well as $f_{\text{peak}}/f_{\text{sig}}$ (9.7%) and $f_{D^*a_1}/f_{\text{sig}}$ (11.6%), are obtained from the Monte Carlo simulation. The kinematic-variable fit to the $B^0 \rightarrow D^{*-} \rho^+$ sample [Figs. 2(a), 2(b) and 2(c)] yields 5520

TABLE I. Summary of the systematic uncertainties on the measured B^0 lifetime.

Source	Errors (ps)	
	$B^0 \rightarrow D^{*-} \pi^+$	$B^0 \rightarrow D^{*-} \rho^+$
(1) Background parameters	0.023	0.044
(2) Monte Carlo statistics	0.021	0.042
(3) Fractional composition	0.008	0.024
(4) D^0 tracks bias	0.017	0.026
(5) Δt resolution model	0.011	0.015
(6) Likelihood fit bias	0.005	0.016
(7) Δt range	0.009	0.009
(8) z scale	0.006	0.007
(9) SVT misalignment	0.008	0.008
(10) Beam energies	0.002	0.002
Total	0.041	0.075

$\pm 250 B^0 \rightarrow D^{*-} \rho^+$ events, including 691 ± 36 fully reconstructed events.

In the second step, all the parameters determined in the first step are fixed, and the parameters of $\mathcal{F}_i(\Delta t, \sigma_{\Delta t})$ of the backgrounds are determined entirely from the control data samples. In the $B^0 \rightarrow D^{*-} \pi^+$ case, the parameters of $\mathcal{F}_{\text{cont}}(\Delta t, \sigma_{\Delta t})$ are obtained from a fit to the $B\bar{B}$ -depleted sample, and those of the $\mathcal{F}_{\text{comb}}(\Delta t, \sigma_{\Delta t})$ are obtained from the same-charge sample. The parameters of $\mathcal{F}_{\text{peak}}(\Delta t, \sigma_{\Delta t})$ are assumed to be identical to $\mathcal{F}_{\text{comb}}(\Delta t, \sigma_{\Delta t})$. In $B^0 \rightarrow D^{*-} \rho^+$, the parameters of $\mathcal{F}_{\text{comb}}(\Delta t, \sigma_{\Delta t})$ are determined from the sideband sample, and those of $\mathcal{F}_{\text{peak}}(\Delta t, \sigma_{\Delta t})$ are obtained from the same-charge sample. Each of the $B^0 \rightarrow D^{*-} \rho^+$ control sample fits is conducted simultaneously on the on- and off-resonance data, and the parameters of $\mathcal{F}_{\text{cont}}(\Delta t, \sigma_{\Delta t})$ are determined for each control sample simultaneously with the $B\bar{B}$ PDF parameters. All use of control samples and corresponding assumptions was validated using the Monte Carlo simulation.

In the final step, using the background $\mathcal{F}_i(\Delta t, \sigma_{\Delta t})$ parameters obtained in the previous step, the signal region sample is fit to extract the signal $\mathcal{F}_{\text{sig}}(\Delta t, \sigma_{\Delta t})$ parameters. In $B^0 \rightarrow D^{*-} \pi^+$ this fit has six free parameters describing $\mathcal{F}_{\text{sig}}(\Delta t, \sigma_{\Delta t})$. In $B^0 \rightarrow D^{*-} \rho^+$, the fit is done simultaneously to on- and off-resonance events, as well as fully reconstructed events, and has 15 free parameters describing $\mathcal{F}_{\text{sig}}(\Delta t, \sigma_{\Delta t})$ and $\mathcal{F}_{\text{cont}}(\Delta t, \sigma_{\Delta t})$.

The results of the last fit step, shown in Figs. 1(b) and 2(d), are $\tau_{B^0} = 1.510 \pm 0.040$ ps for $B^0 \rightarrow D^{*-} \pi^+$ and $\tau_{B^0} = 1.616 \pm 0.064$ ps for $B^0 \rightarrow D^{*-} \rho^+$, where the errors are statistical only. These results are obtained after a correction of -0.014 ± 0.020 ps ($+0.071 \pm 0.028$ ps for $B^0 \rightarrow D^{*-} \rho^+$), determined from the Monte Carlo simulation. The correction accounts for biases due to the fit procedure, the event selection and, in the $B^0 \rightarrow D^{*-} \rho^+$ case, the effect of \bar{D}^0 daughter tracks passing the cone cut and being used for the determination of the other B vertex. The errors in the corrections are propagated to the final result as systematic errors.

The systematic uncertainties are listed in Table I, and de-

scribed here. (1) The fractions and the PDF parameters of the background components were varied by their statistical errors, taking into account mutual correlations, obtained from the fits of the first two analysis steps. (2) The PDF parameters and lifetime corrections that were obtained from the Monte Carlo simulation were varied by the statistical error in the Monte Carlo fits. The full analysis chain, including event reconstruction and selection, was tested with the Monte Carlo simulation, and the statistical precision of the consistency between the generated and fit lifetimes was assigned as a systematic error. The Monte Carlo statistical errors in the evaluation of the various corrections described above were propagated to the final result. (3) The level of $B^0 \rightarrow D^{*-} \rho^+$ ($B^0 \rightarrow D^{*-} a_1^+$) background in the $B^0 \rightarrow D^{*-} \pi^+$ ($B^0 \rightarrow D^{*-} \rho^+$) sample was varied by the relevant branching fraction errors [9], and the fraction of $B \rightarrow D^{*-} \rho^+$ background events in the $B^0 \rightarrow D^{*-} \rho^+$ sample, which is nominally 0, was varied up to 40% of the signal yield. (4) The fraction of events where at least one \bar{D}^0 track satisfies the cone cut was varied by $\pm 5\%$ in the simulated sample, and the associated bias was reevaluated. (5) The parameters of \mathcal{F}_{sig} that were fixed in the fits were varied within conservative ranges. (6) Extensive parametrized Monte Carlo simulation studies were conducted to evaluate statistical biases in the fits due to limited data sample size or as the result of changes in the functional form of $R((\Delta t - \Delta t_{\text{true}})/\sigma_{\Delta t})$. (7) The Δt fit range was varied between $|\Delta t| < 10$ ps and $|\Delta t| < 20$ ps. (8) The z length scale of the detector has been determined with an uncertainty of 0.4% from the reconstruction of secondary interactions with a beam pipe section of known length [15]. The systematic uncertainties related to the detector alignment (9) and beam energy uncertainty [8] (10) were also taken into account. The total systematic error in the $B^0 \rightarrow D^{*-} \pi^+$ ($B^0 \rightarrow D^{*-} \rho^+$) analysis is 0.041 ps (0.075 ps).

Several cross-checks were conducted to demonstrate the validity of the result. The data were fit in bins of the lab frame polar angle, azimuthal angle, and momentum of the π_h , and in subsamples corresponding to different SVT alignment calibrations. The fit was repeated with different values of the cone cut ranging from 0.75 to 2.00 radians (0.6 to 1.2 radians for $B^0 \rightarrow D^{*-} \rho^+$). Different functional forms of $R((\Delta t - \Delta t_{\text{true}})/\sigma_{\Delta t})$ were used in the fit. In all cases, no statistically significant variation of the result was observed, beyond those already accounted for in the systematic errors.

In summary, in a sample of 22.7 million $B\bar{B}$ pairs, we identify $6970 \pm 240 B^0 \rightarrow D^{*-} \pi^+$ and $5520 \pm 250 B^0 \rightarrow D^{*-} \rho^+$ partially reconstructed decays. These events are used to measure the B^0 lifetime, obtaining $\tau_{B^0} = 1.510 \pm 0.040$ (stat) ± 0.041 (syst) ps in $B^0 \rightarrow D^{*-} \pi^+$ and $\tau_{B^0} = 1.616 \pm 0.064$ (stat) ± 0.075 (syst) ps in $B^0 \rightarrow D^{*-} \rho^+$. The combined measurement, taking into account correlated errors, is

$$\tau_{B^0} = 1.533 \pm 0.034 \text{ (stat)} \pm 0.038 \text{ (syst) ps.}$$

This result is in good agreement with the world average B^0 lifetime $\tau_{B^0} = 1.542 \pm 0.016$ ps [9] and with other recent

BABAR measurements [16], confirming the validity of using partially reconstructed events in time dependent measurements.

We are grateful for the excellent luminosity and machine conditions provided by our PEP-II colleagues, and for the substantial dedicated effort from the computing organizations that support *BABAR*. The collaborating institutions

wish to thank SLAC for its support and kind hospitality. This work is supported by DOE and NSF (USA), NSERC (Canada), IHEP (China), CEA and CNRS-IN2P3 (France), BMBF and DFG (Germany), INFN (Italy), NFR (Norway), MIST (Russia), and PPARC (United Kingdom). Individuals have received support from the A. P. Sloan Foundation, Research Corporation, and Alexander von Humboldt Foundation.

-
- [1] Charge conjugate decays are implied.
- [2] R. G. Sachs, Enrico Fermi Institute Report, EFI-85-22, 1985; I. Dunietz and R. G. Sachs, *Phys. Rev. D* **37**, 3186 (1988); **39**, 3515(E) (1989); I. Dunietz, *Phys. Lett. B* **427**, 179 (1998); *BABAR* Physics Book, edited by P. F. Harrison and H. R. Quinn (1998), Chap. 7.6; D. London, N. Sinha, and R. Sinha, *Phys. Rev. Lett.* **85**, 1807 (2000).
- [3] N. Cabibbo, *Phys. Rev. Lett.* **10**, 531 (1963); M. Kobayashi and T. Maskawa, *Prog. Theor. Phys.* **49**, 652 (1973).
- [4] CLEO Collaboration, G. Brandenburg *et al.*, *Phys. Rev. Lett.* **80**, 2762 (1998).
- [5] *BABAR* Collaboration, B. Aubert *et al.*, hep-ex/0203038.
- [6] *BABAR* Collaboration, B. Aubert *et al.*, hep-ex/0203036.
- [7] "GEANT, Detector Description and Simulation Tool," CERN program library long writeup W5013, 1994.
- [8] *BABAR* Collaboration, B. Aubert *et al.*, *Nucl. Instrum. Methods Phys. Res. A* **479**, 1 (2002).
- [9] Particle Data Group, K. Hagiwara *et al.*, *Phys. Rev. D* **66**, 010001 (2002).
- [10] Unless explicitly noted, the value or procedure in the text refers to the $B^0 \rightarrow D^{*-} \pi^+$ analysis while those in parentheses refer to the $B^0 \rightarrow D^{*-} \rho^+$ analysis.
- [11] G. Fox and S. Wolfram, *Phys. Rev. Lett.* **41**, 1581 (1978).
- [12] π_h denotes both the charged pion from the ρ decay in $B^0 \rightarrow D^{*-} \rho^+$ and the hard pion from $B^0 \rightarrow D^{*-} \pi^+$.
- [13] R. A. Fisher, *Ann. Eugenics* **7**, 179 (1936); M. S. Srivastava and E. M. Carter, *An Introduction to Applied Multivariate Statistics* (North-Holland, Amsterdam, 1983).
- [14] ARGUS Collaboration, H. Albrecht *et al.*, *Phys. Lett. B* **254**, 288 (1991).
- [15] *BABAR* Collaboration, B. Aubert *et al.*, *Phys. Rev. D* **66**, 032003 (2002).
- [16] *BABAR* Collaboration, B. Aubert *et al.*, *Phys. Rev. Lett.* **87**, 201803 (2001); *BABAR* Collaboration, B. Aubert *et al.*, *ibid.* **89**, 011802 (2002).